Streamers feeding the SVS13-A protobinary system: astrochemistry reveals accretion shocks?
Bianchi, E.; Lopez-Sepulcre, A.; Ceccarelli, C.; Codella, C.; Podio, L.; Bouvier, M.M.E.; ... ; Lefloch, B.

Faraday Discussions

Cite this: *Faraday Discuss.*, 2023, **245**, 164

PAPER

Streamers feeding the SVS13-A protobinary system: astrochemistry reveals accretion shocks?

Eleonora Bianchi, [*a] Ana López-Sepulcre, [bc] Cecilia Ceccarelli, [b] Claudio Codella, [db] Linda Podio, [d] Mathilde Bouvier, [e] Joan Enrique-Romero, [f] Rafael Bachiller [g] and Bertrand Lefloch [bh]

Received 27th January 2023, Accepted 16th March 2023

DOI: 10.1039/d3fd00018d

We report Atacama Large Millimeter/submillimeter Array (ALMA) high-angular resolution (∼50 au) observations of the binary system SVS13-A. More specifically, we analyse deuterated water (HDO) and sulfur dioxide (SO_2) emission. The molecular emission is associated with both the components of the binary system, VLA4A and VLA4B. The spatial distribution is compared to that of formamide (NH_2CHO), previously analysed in the system. Deuterated water shows an additional emitting component spatially coincident with the dust-accretion streamer, at a distance ≥120 au from the protostars, and at blue-shifted velocities (>3 km s^{-1} from the systemic velocities). We investigate the origin of the molecular emission in the streamer, in light of thermal sublimation temperatures calculated using updated binding energy (BE) distributions. We propose that the observed emission is produced by an accretion shock at the interface between the accretion streamer and the disk of VLA4A. Thermal desorption is not completely excluded in case the source is actively experiencing an accretion burst.

[a]*Excellence Cluster ORIGINS, Boltzmannstraße 2, Garching bei München, 85748, Germany. E-mail: eleonora.bianchi@origins-cluster.de*

[b]*Univ. Grenoble Alpes, CNRS, IPAG, 38000 Grenoble, France*

[c]*Institut de Radioastronomie Millimétrique, 38406 Saint-Martin d' Hères, France*

[d]*INAF, Osservatorio Astrofisico di Arcetri, Largo E. Fermi 5, Firenze, I-50125, Italy*

[e]*Leiden Observatory, Leiden University, P.O. Box 9513, 2300 RA Leiden, The Netherlands*

[f]*Leiden Institute of Chemistry, Gorlaeus Laboratories, Leiden University, P.O. Box 9502, 2300 RA Leiden, The Netherlands*

[g]*Observatorio Astronómico Nacional (OAN-IGN), Alfonso XII 3, 28014 Madrid, Spain*

[h]*Laboratoire d'astrophysique de Bordeaux, Univ. Bordeaux, CNRS, B18N, Allée Geoffroy Saint-Hilaire, 33615 Pessac, France*

1 Introduction

Our understanding of how a star and a planetary system form has evolved substantially in recent years. On the one hand, observations have revealed the presence of substructures, such as gaps and rings, in very young protostellar disks (age $\sim 10^5$ years).[2–4] On the other hand, evolved Class II disks (age > 10^6 years) do not contain enough dust mass to explain the observed exoplanet population, in contrast to early Class 0 and I disks, which are more massive.[5] These indications suggest that planetesimal formation has started already in the early phases of protostellar disks. In this respect, it is of paramount importance to investigate the properties of young Class 0 (age $\sim 10^4$ years) and Class I disks (age $\sim 10^5$ years) in order to define the initial conditions for planet formation. Since young disks are typically deeply embedded in the parent envelope, the characterisation of their physical and chemical properties is not trivial from an observation point of view. If simple parameters, such as the disk dust and gas mass, are already difficult to measure (see *e.g.* ref. 6 and 7), their chemical composition is even less explored. Nevertheless, the molecular complexity present in the disk will be inherited from the forming planets, at least in the outer regions (see *e.g.* ref. 8 and 9 and references therein). Shedding light on the chemical composition of young disks is the only way to investigate the initial chemical budget available for planets when they start to form. Because of an important envelope contribution, the standard gas tracers (*e.g.* CO isotopologues) fail in the observation of the inner disk regions of young protostars. Other tracers, such as interstellar complex organic molecules (iCOMs; molecules with 6 or more atoms and based on carbon; see *e.g.* ref. 9 and 10) have been demonstrated to be more effective in studying the complex processes happening in the disk. However, their employment requires, at the same time, sensitive observations and a better understanding of the chemical/physical processes that release the molecules we observe in the gas. In this context, a strong synergy between astronomical observations, quantum chemistry calculations and laboratory experiments is required. In this paper, we present new observations of the protobinary system SVS13-A performed using the Atacama Large Millimeter/submillimeter Array (ALMA). In section 2 we present the source background and in section 3 we describe the ALMA observations. The main results of our analysis are presented in section 4. Section 5 discusses the possible origin of the detected molecular emission, using the most up-to-date binding-energy distributions. The main conclusions are reported in section 6.

2 The protostellar binary system SVS13-A

SVS13-A is a perfect target on which to perform astrochemical studies and tackle some of the questions above. It is very well studied, and is located in Perseus, at a distance of ~299 pc (*Gaia*[11]). The system has a bolometric luminosity of 58.8 $L_\odot$,[12] and it is at the origin of the famous Herbig–Haro (HH) chain 7–11,[13] a molecular jet and a large-scale outflow.[14,15] SVS13-A is composed of a close binary system with a separation of 0.3″.[16] The proper motion of the two components, VLA4A and VLA4B, has been investigated for almost 30 years.[17,18] A third companion, called SVS13A2, is detected at a distance of ~5″.[19,20] The continuum emission at high-angular resolution shows two circumstellar disks and circumbinary material distributed in spiral arms, which suggest accretion streamers (see Fig. 1).[1,18,20] More specifically, a bright arc is observed from the position of VLA4A extending towards the south-east. Two other arcs are extending from VLA4B towards the east and west sides of VLA4A. In addition, we detect three elongated structures that extend from the northern edge of the continuum associated with VLA4A and B towards the north. For simplicity, later in the text we refer to the central arc-like structure as the northern streamer. In order to verify that these structures are not artifacts introduced by the cleaning process, we test different beam tapering. All the elongated arc-like structures are still present when using a larger circular beam. We conclude that the dust emission is tracing accretion streamers extending towards the north and the south and feeding VLA4A and VLA4B.

The optical source position measured using *Gaia* is very close to VLA4B, even though there is a non-negligible discrepancy suggesting that the protostar is very embedded and the optical emission is due to light scattered by the circumbinary material.[18] The source driving the molecular jet, as well as a microjet traced by [Fe II], has also been identified for VLA4B.[15,21] When observed at mm wavelengths, VLA4B is brighter than VLA4A by a factor of 3.8 at 7 mm and 3.7 at 9 mm,[16] while the flux becomes comparable at longer wavelengths.[5,20] The situation reverses at 1.2 mm where VLA4A is brighter by a factor of 1.5.[1] The analysis of spectral energy distribution (SEDs) reveals the presence of free–free emission for both VLA4A and VLA4B, consistent with the presence of radio jets.[18] The different spectral indices measured toward the sources, as well as the change in intensities, suggest that the dust at 1.2 mm is optically thick in VLA4A and very optically thick in VLA4B.[5,18] In this

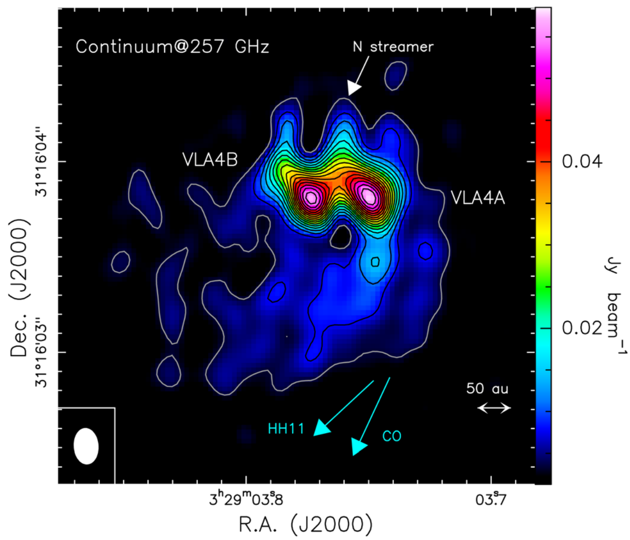

Fig. 1 Continuum emission as observed by ALMA at 1.2 mm (color scale and contours).[1] The first contours (gray) and steps (black) are 8σ, corresponding to 3.35 mJy per beam. The beam size is 0″19 × 0″13 (PA = +5°). The binary system is composed of VLA4A (right) and VLA4B (left). The coordinates are α_{J2000} = 03^h 29^m 3.75^s, δ_{J2000} = +31° 16′ 03.81″ and α_{J2000} = 03^h 29^m 3.773^s, δ_{J2000} = +31° 16′ 03.81″ for VLA4A and VLA4B, respectively. The blue arrows indicate the directions toward HH11 (133°) as well as the main axis of the H_2/CO jet (155°), as inferred by Lefèvre *et al.*[15] The white arrow indicates the position of the northern streamer discussed in the text.

context, VLA4B is interpreted as the primary and more massive component of the binary system, while VLA4A would be the less evolved secondary component. Taking into account the high uncertainties related to the free–free contamination, the disk masses have been estimated to be ~0.2 $M_\odot$ for VLA4B and ~0.08 $M_\odot$ for VLA4A,[5] confirming this picture. Interestingly, SVS13-A has also been deeply investigated in the NIR and found to be in a phase of active accretion.[12] The quick rise of magnitude in the K-band, followed by a slow decline, is reminiscent of FU Ori sources, while the small bursts amplitude and the line-rich spectra resemble EX Ori sources.[21]

2.1 The prototype Class I hot corinos

SVS13-A has been found to host hot corino chemistry. More specifically, young Class 0 protostars possess an inner region, typically ≤100 au, where the gas temperature is high enough (≥100 K) to desorb the icy mantles of dust grains and release complex molecules into the gas phase, which can in turn react in the gas phase and form more complex molecular species. The hot corino phenomenon was first observed in Class 0 protostars (*e.g.* IRAS16293-2422 (ref. 22)) and only recently it was also discovered in more evolved Class I objects. In this respect, SVS13-A provided the first evidence that Class I objects can be as chemically rich as young Class 0 sources.[23] More specifically, water and iCOM emission have been detected from a compact (<100 au) and hot (>100 K) region[23–25] towards the source. Since then, the chemistry of the system has been deeply investigated thanks to several observational Large Programs including ASAI (Astrochemical Surveys At IRAM 30 m [26]), CALYPSO (Continuum and Lines in Young ProtoStellar Objects[27]) with the Plateau de Bure interferometer, SOLIS (Seed Of Life In Space[28]) with IRAM-NOEMA and PEACHES (Perseus ALMA Chemistry Survey[29]). These projects identified more than 100 emission lines emitted by iCOMs, including those of CH_3OH and its isotopologues, CH_3CHO, $HCOOCH_3$, CH_3OCH_3, $HCOCH_2OH$, NH_2CHO and CH_3-CH_2OH. The broad spectral coverage of these surveys allowed a detailed multi-line analysis, which results in an accurate determination of the gas properties. In particular, rotational temperatures and column density of each molecule have been determined and compared to those measured in other objects. The relative iCOM abundances are in good agreement with measurements both in Class 0 protostars and in the 67P/Churyumov–Gerasimenko comet, suggesting to some extent inheritance of complexity from the early stages.[23] ALMA high-angular resolution observations (~50 au) shed new light on the distribution of iCOMs across the binary system. In particular, a striking chemical segregation was observed. Some molecular species, such as methanol and dimethyl ether, are detected in both VLA4A and VLA4B, while others, *e.g.* formamide and ethylene glycol, are detected only in VLA4A.[1,18] Interestingly, the line emission appears to be elongated towards the north (up to ~150 au), where one of the accretion streamers in the dust is present (see Fig. 1). The origin of such a molecular line distribution needs to be clarified using different molecular tracers. For this purpose, we report here the analysis of sulfur dioxide (SO_2) and deuterated water (HDO) in the SVS13-A system.

3 Observations

The observations presented here were acquired using the Atacama Large Millimeter/submillimeter Array (ALMA) on 8 September 2019 during the project

Table 1 List of transitions and line properties (on the T_{MB} scale) of the HDO, SO_2 and NH_2CHO emission. The columns report the transitions and their frequency ν (GHz), the upper-level energy E_{up} (K), the line strength $S\mu^2$ (D^2), the velocity-integrated line intensity I_{int} (mK km s^{-1}) and the intensity ratio

Species	Transition	ν^a (GHz)	$E_{up}{}^a$ (K)	$S\mu^{2a}$ (D^2)	$I_{int}{}^b$ (mK km s^{-1}) VLA4A	$I_{int}{}^b$ (mK km s^{-1}) VLA4B	Intensity ratio VLA4A/VLA4B
HDO	2(1,1)–2(1,2)	241.561550	95	0.4	349 (70)	177 (36)	2.0 (0.6)
$SO_2{}^c$	5(2,4)–4(1,3)	241.615797	24	5.7	≥126	≥175	—
NH_2CHO^d	12(1,12)–11(1,11)	243.521044	79	156	267 (59)	40 (11)	7 (2)

[a] Frequencies and spectroscopic parameters have been taken from ref. 31 for HDO, and retrieved from the Jet Propulsion Laboratory molecular database (**https://spec.jpl.nasa.gov/**).[32] For NH_2CHO, spectroscopic parameters are taken from ref. 34 and retrieved from the Cologne Database for Molecular spectroscopy (**https://cdms.astro.uni-koeln.de/**).[33] [b] Errors on the integrated intensity include 20% calibration uncertainty. [c] Contaminated by the CH_2DOH ($4_{3,1}$–$5_{1,5}$)e1 line at 241.61928840 GHz, at −4.3 km s^{-1} from the SO_2 rest line. [d] From ref. 1.

(2018.1.01461.S, see also ref. 1). The telescope was in the C43-6 configuration, with baselines between 43 m and 5.9 km. The center of the observed field is $\alpha_{J2000} = 03^h\,29^m\,3.8^s$, $\delta_{J2000} = +31°\,16'\,03.8''$. The bandpass and flux calibrator was the quasar J0510 + 1800, while the phase calibrator was J0336 + 3218. Data calibration was performed using the standard ALMA calibration pipeline in CASA.[30] Successively, we used the IRAM-GILDAS† package to determine line-free continuum channels, perform phase self-calibration and apply the solution both to the continuum and the spectral cubes. The final calibration uncertainty on the absolute flux is 20%.

4 Results

We detect and analyse the HDO 2(1,1)–2(1,2) transition at 241.561550 GHz with an upper-level energy (E_{up}) of 95 K. In the same spectral window we also detect the SO_2 5(2,4)–4(1,3) transition at 241.615797 GHz with E_{up} of 24 K. The line spectroscopic parameters are listed in Table 1. The rms (root mean square) noise is typically 4.8 mJy per beam km s^{-1} using spectral channels of 122 kHz (0.15 km s^{-1}). The synthesized beam is $0.21'' \times 0.14''$ for both the line cubes. The analysis is supported by the NH_2CHO 12(1,12)–11(1,11) transition at 243.521044 GHz, previously published in ref. 1.

Fig. 2 shows the spatial distribution of the HDO (left panel), NH_2CHO (middle panel) and SO_2 (right panel) lines with respect to the dust continuum emission. In particular, the line emission is integrated over the whole velocity interval and reported in a color scale superposed to the continuum emission shown as white contours. As already noticed in ref. 1, the NH_2CHO emission is more compact and centered in VLA4A, while HDO and SO_2 have a broader emission, extending also towards VLA4B. This finding confirms the chemical segregation reported in the

† **https://www.iram.fr/IRAMFR/GILDAS**.

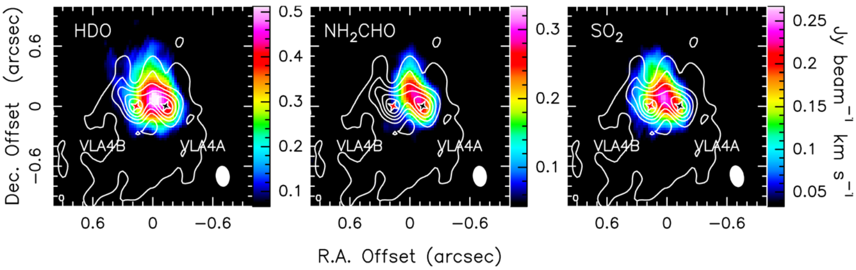

Fig. 2 Velocity-integrated emission (moment 0) of the HDO 2(1,1)–2(1,2) (left panel), NH_2CHO 12(1,12)–11(1,11) (middle panel) and SO_2 5(2,4)–4(1,3) (right panel) lines, in a colour scale, superposed to the dust emission shown as white contours. The synthesised beams are shown in white in the lower right corner of each panel. The black and red stars indicate the VLA4A and VLA4B positions, respectively.

binary system using iCOMs.[1,18] Moreover, HDO and SO_2 emissions show an elongation toward the north, as already observed for iCOMs.

In order to further investigate the lines' radial and vertical distributions, we plot in Fig. 3 the intensity [Jy] profiles of SO_2, HDO and NH_2CHO extracted from the moment 0 maps (see Fig. 2) along a horizontal axis connecting the two protostars (left panel) and a vertical axis between the protostars, crossing the northern streamer (right panel). The x-axis reports the offset in astronomical units with respect to the position of VLA4A. The vertical dashed lines indicate the positions of the two protostars. The radial profiles show that HDO and SO_2 are extended in a region covering both protostars with a peak of emission in between. Despite the difference in the peak intensity, there are no substantial differences between the spatial distributions of HDO and SO_2. Conversely, NH_2CHO has

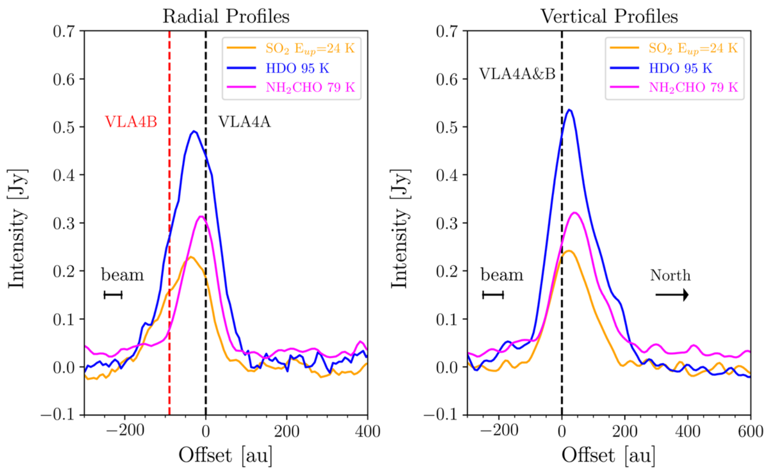

Fig. 3 Left panel: Intensity profile of the HDO line at 241.56155 GHz (blue) and the SO_2 line at 241.615797 GHz (orange) extracted along a line connecting VLA4A with VLA4B. The two vertical dashed lines show the positions of VLA4A (black) and VLA4B (red). Right panel: Intensity profile of the same lines extracted along a vertical line crossing the northern streamer. The vertical dashed line shows the position of VLA4A and VLA4B.

a peak of the emission closer to VLA4A.[1] In addition, the vertical profiles show that all the molecules are extended toward the north direction at a larger distance than the dust streamer, located at ~0.4″ (corresponding to 120 au at the source distance). The radial and vertical profiles do not show a trend with the upper level energy of the different lines, confirming that the molecular distributions do not strongly depend on the excitation conditions.[1]

We report in Table 1 the integrated line intensities extracted from the continuum peak positions of VLA4A and VLA4B, respectively, and their intensity ratios. The intensity ratio for HDO is 2.0 (0.6), suggesting that water is distributed in both the protostars, even if it is more abundant in VLA4A. Similar intensity ratios were derived for iCOMs such as CH_3OH and CH_3CHO.[1] On the other hand, the intensity ratio measured for the NH_2CHO line is 7 (2), confirming the presence of formamide predominantly towards VLA4A. We also report the intensity of SO_2

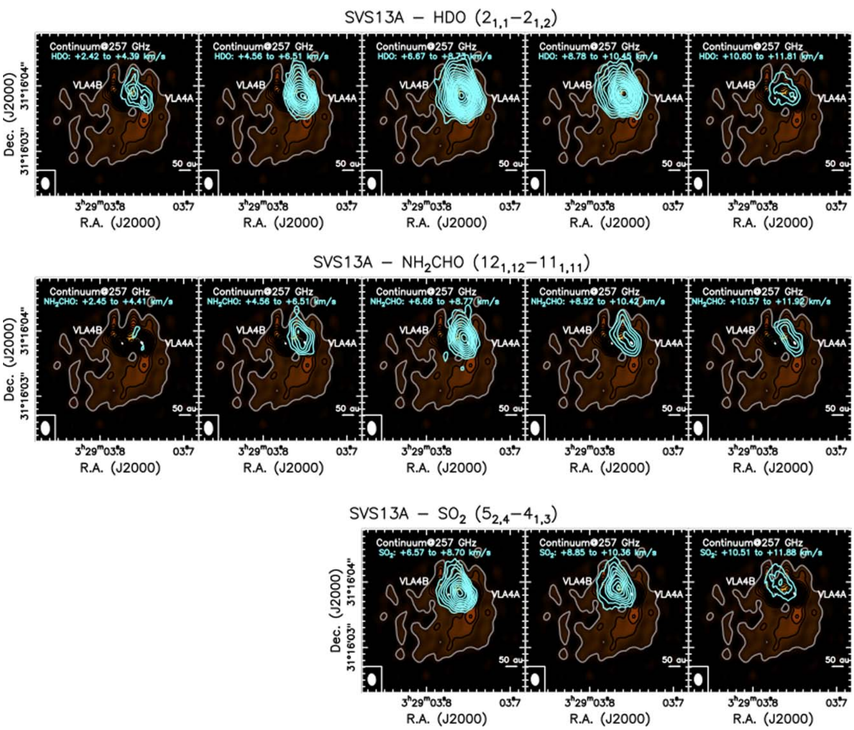

Fig. 4 Upper panels: Channel map of the HDO($2_{1,1}$–$2_{1,2}$) emission (cyan contours) overlapped on the 1.2 mm continuum map of SVS13-A VLA4A and VLA4B (see Fig. 1). Five velocity intervals have been considered (reported in the top-left corner of each panel). The first contours and steps correspond to 5σ (20 mJy per beam km s^{-1} for all the channels but the most blue- and red-shifted ones, with 16 mJy per beam km s^{-1}), and 2σ, respectively. The systemic velocities are +7.7 km s^{-1} (VLA4A) and +8.5 km s^{-1} (VLA4B). The synthesised beam (bottom-left of each panel) is 207 × 136 mas (PA = +5°). Middle panels: Same as the upper panels, for NH_2CHO ($12_{1,12}$–$11_{1,11}$). First contours and steps as for HDO. Lower panels: Same as the upper panels, for SO_2 ($5_{2,4}$–$4_{1,3}$). First contours and steps as for HDO. In this case, only three velocity intervals can be drawn because of the contamination due to the CH_2DOH($4_{3,1}$–$5_{1,5}$)e1 line at 241.61928840 GHz, *i.e.* at −4.3 km s^{-1} from the SO_2 rest line (see Table 1).

in VLA4A and VLA4B. The ratio is not reported in this case since the blue-shifted part of the line is contaminated and the line intensity extracted for VLA4A is a lower limit. The HDO line intensity of the brighter source, VLA4A, is consistent with the rotational temperature of 150–260 K and a column density of 4×10^{17} cm^{-2}, derived using IRAM-30 m data considering the emission from both protostars.[24] The NH_2CHO rotational temperatures and column densities derived in ref. 1 are $T_{rot} = 140$ K and $N_{tot} = 5.9(0.9) \times 10^{15}$ cm^{-2} in VLA4A and $T_{rot} = 170$ K and $N_{tot} = 1.4(0.3) \times 10^{15}$ cm^{-2} in VLA4B.

Fig. 4 shows the spatial distributions of HDO (upper panels), NH_2CHO (middle panels) and SO_2 (lower panels) with respect to the dust continuum emission. More specifically, the line emission is integrated in five different velocity channels and showed with cyan contours superposed to the continuum emission in a color scale. The NH_2CHO emission in all the velocity intervals traces only VLA4A and it is elongated toward the northern streamer. For HDO, the blue-shifted emission in the velocity intervals 2.4–4.4 km s^{-1} and 4.6–6.5 km s^{-1} shows the same distribution. In the velocity intervals 6.7–8.7 km s^{-1}, 8.8–10.5 km s^{-1} and 10.6–11.8 km s^{-1} the line emission is associated with both protostars, peaking in between. The central panels correspond to the systemic velocities of VLA4A and VLA4B, which are +7.7 km s^{-1} and +8.5 km s^{-1}, respectively, and have been determined from methanol emission.[1] SO_2 emission is also associated with both protostars in the velocity intervals 6.6–8.7 km s^{-1}, 8.9–10.4 km s^{-1}, and 10.5–11.9 km s^{-1}. Even if the blue-shifted part of the line (velocities lower than +6.5 km s^{-1}) is contaminated by the $CH_2DOH(4_{3,1}–5_{1,5})$e1 line at 241.61928840 GHz (see Table 1), the SO_2 emission in the other available channels shows a spatial distribution similar to that of HDO. The overall line distribution confirms what was previously reported in ref. 1, but the HDO emission highlights an additional structure (i) with a peak spatially shifted with respect to the protostar position, and (ii) at velocities blue-shifted by $\geq$3 km s^{-1}. This component is perfectly aligned with the northern streamer traced by the dust, thus revealing molecular gas associated with the streamer itself. Interestingly, in the same blue-shifted velocity range, NH_2CHO shows hints of this component even if the S/N is lower than that of HDO (see Fig. 3).

5 Discussion

5.1 Binding energies and sublimation temperatures

As we will discuss in more detail in the next subsection, the presence of deuterated water, SO_2 and formamide in the gas phase provides new insights into their origin.

First, deuterated water is prevalently formed in the cold prestellar phase on grain surfaces, in the so-called mantle (see *e.g.* ref. 35). Therefore, HDO remains frozen unless it is released into the gas phase by some process. In general, two processes can possibly inject HDO into the gas phase (*e.g.* see the discussion in ref. 9): the thermal sublimation from warm dust grains or a (non-thermal) shock. Other possible mechanisms, such as chemical desorption or photo-desorption, would not be efficient here. Concerning formamide, there has been some discussion on its formation route. In principle, it can be synthesised on grain surfaces (see *e.g.* ref. 36) or in the gas phase[37] from reactants (H_2CO and NH_2) that are formed on grain surfaces, or both. If formed on grain surfaces, formamide would need to be released into the gas phase by either thermal sublimation or a (non-thermal) shock, as HDO. The same consideration applies if formamide is formed in the gas phase, because the two reactants H_2CO and NH_2 would need to be in the gaseous form. Finally, SO_2 is formed in the gas phase, but sulfur is observed to be depleted, by about a factor of 20, in cold molecular clouds,[38] so it is often taken as a tracer of warm and shocked regions. In summary, the presence of HDO, SO_2 and NH_2CHO implies that either they (or their precursors) are thermally sublimated or they are injected from the frozen mantles into the gas phase by a shock.

In order to distinguish which of the two hypotheses is correct, one has to evaluate the thermal sublimation temperature of deuterated water, SO_2 and formamide. To this end, we used the half-life time t_{sub} of the frozen species:

$$t_{sub} = \ln(2)/k_{des} \tag{1}$$

The rate of desorption k_{des} is given by the usual equation:

$$k_{des} = \nu_{des}\exp(-BE/T) \tag{2}$$

where BE is the binding energy, given in units of temperature, and ν_{des} is the pre-exponential factor, which depends on the adsorbate and surface (see *e.g.* ref. 39 and 40).

Table 2 lists the BEs of HDO, SO_2 and NH_2CHO over an amorphous water surface, as computed in ref. 41 and 42 on a ice model of 60 water molecules. Note that the HDO BE was assumed to be equal to that of H_2O, an assumption demonstrated to be valid by new computations by Tinacci *et al.* (submitted) on a large (200 molecules) water-ice grain. The table also reports the pre-exponential factors ν of H_2O and NH_2CHO, computed in ref. 39 following the formalism in ref. 43 (see Table 5 of ref. 39). The pre-exponential factor of SO_2 was estimated by us using the formalism in ref. 43.

Fig. 5 shows the derived sublimation temperatures of deuterated water and formamide, for a time interval between 10^3 and 10^5 years. We do not show the case of SO_2 for clarity reasons, since its sublimation temperature would lie below that of HDO. The figure shows three sublimation temperature curves for each species, corresponding to the average, minimum and maximum BEs computed in ref. 41. Assuming that, in reality, the BE has a distribution of values approximately described by a Gaussian function (see *e.g.* ref. 45), the curve corresponding to the average would represent where most of the relevant molecules would thermally sublimate. While HDO being in the gaseous form is, in principle (see below), compatible with thermal sublimation, the same is not

Table 2 Binding energies (BEs) and pre-exponential factors (ν) used for deriving the sublimation temperatures shown in Fig. 5. The BEs are from ref. 41 and 42. The pre-exponential factors are from ref. 39 (see text). Note that the second column reports minimum and maximum values of BE computed on a amorphous water surface model of 60 molecules. The third column reports the pre-exponential factors computed using the method in ref. 43, also described and discussed in ref. 39 and 40

Species	BE [K]	ν [s^{-1}]
HDO	3605–6111	5×10^{15}
SO_2	2105–5827	2×10^{16}
NH_2CHO	5793–10 960	4×10^{18}

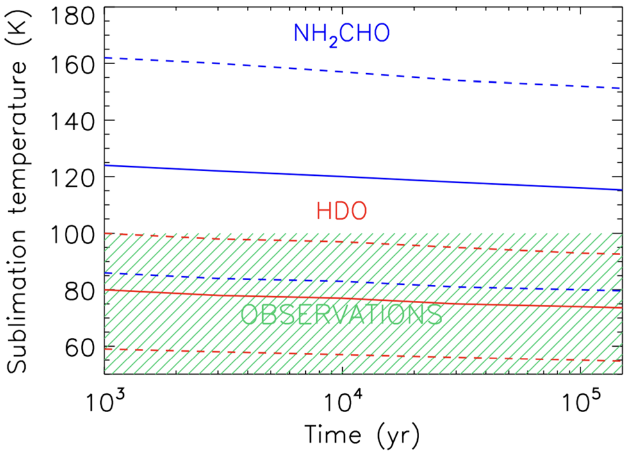

Fig. 5 Sublimation temperatures of deuterated water (HDO; red lines) and formamide (NH_2CHO; blue lines). The three curves for each species correspond to the average (solid line), minimum and maximum (dashed lines) BEs computed in ref. 41 and reported in Table 2 (see text). Note that for HDO we used the same BE as H_2O, as demonstrated to be valid by Tinacci *et al.* (submitted). The green area shows the grain temperature derived in ref. 44 assuming a bolometric luminosity of 55 $L_\odot$ and a distance from the center of 120 au (see text).

true for formamide. The implications of this fact will be discussed in the following subsection.

5.2 Accretion streamers feeding the disks

The bolometric luminosity (L_{bol}) of VLA4A and VLA4B is not measured singularly due to angular resolution limitations at infrared wavelengths. The total bolometric luminosity of VLA4A + VLA4B is estimated to be in the range 45–55 $L_\odot$,[20,46] at the source distance of 299 pc. The dust streamer traced by the continuum emission extends at a distance larger than 0.4″ (120 au). If we consider a spherical envelope-like distribution, and conservatively a bolometric luminosity of 55 $L_\odot$, the temperature at this distance from the protostars is lower than 100 K (see *e.g.* ref. 47). The presence of formamide at this position, considering the information on the binding energies and the corresponding sublimation temperatures (see section 5.1 and Fig. 5), suggests that formamide is not thermally desorbed. In the case of HDO and SO_2, the binding energies are lower, so their presence cannot exclude thermal desorption. If the continuum emission around the protostars originates from an inclined disk (instead of a spherical envelope), as suggested by the observed geometry,[18] the snowlines of NH_2CHO, HDO, and SO_2, would be even closer to the source. Therefore, the detection of molecules at a distance of ≥120 au would exclude the thermal evaporation scenario.

However, episodic accretion is a common process in young stellar objects. More specifically, observations performed using the Very Large Telescope indicate that SVS13-A is in a phase of active accretion, deriving a mass accretion rate of a few 10^{-6} $M_\odot$ per year[12] (see also ref. 48). The presence of an accretion burst is in principle expected to move the snowlines outwards and inject into the gas phase the molecules stored in the dust mantles, as in the case of the Fu Ori V833 disk.[49] However, at near-IR wavelengths VLA4A is not detected,[21] suggesting a negligible contribution to the bolometric luminosity, which will instead be dominated by VLA4B.[12] This is consistent with VLA4B being the primary and more massive component of the binary system, while VLA4A would be the less massive secondary component. The process of differential accretion in a binary system has been studied using numerical simulations and the secondary component is expected to accrete most of the gas, except in the case of very eccentric orbits (see *e.g.* ref. 50 and 51). In this scenario, VLA4A would be the component actively accreting, and the associated accretion burst may be at the origin of the detected molecular emission associated with VLA4A. In order to definitely exclude the possibility that thermal sublimation is responsible for the chemical enrichment at distances larger than 120 au, it is crucial to have an estimate of the individual VLA4A and VLA4B luminosities.

Alternatively, the emission may be produced by an accretion shock, sputtering the grains, occurring when the accretion streamer impacts the disk of VLA4A. This would also justify the fact that the molecular emission shows emission at both blue-shifted and red-shifted velocities in the streamer (see Fig. 4), which may be due to the velocity dispersion caused by the shock. Indeed, a similar scenario has been proposed to explain SO and SO_2 emission, where molecular streamers impact onto the disks in Class I/II sources, observed by the ALMA-DOT project.[52] Also, in these sources we observe both blue-shifted and red-shifted SO and SO_2 emission at the impact region.

Recently, the possible presence of accretion shocks or self-gravitating substructures (see *e.g.* ref. 53) has been invoked to explain local temperature enhancements in the circumbinary material of the Class 0 source IRAS16293-2422.[54] However, in the case of SVS13-A the circumstellar disks around VLA4A and VLA4B, as well as the circumbinary material, are expected to be stable against local gravitational instabilities, as found in ref. 18.

In summary, a major result of the presented observations is the detection of molecular gas in the accretion streamer feeding the system SVS13-A, on a scale of ∼100–200 au Interestingly, an accretion streamer connecting the source to the outer envelope, up to ∼700 au, has been recently imaged in DCN using the IRAM NOEMA interferometer.[55] The detected DCN streamer is associated with the southern dusty streamer, even though some emission is also present in the northern region (see Fig. C.1 in ref. 55). However, the limited angular resolution of the NOEMA observations (synthesized beam of $1.2'' \times 0.7''$) prevents a proper comparison with the ALMA continuum emission. Finally, the present observations confirm that deuterated water and iCOMs, including formamide, are as effective as classical tracers, such as SO and SO_2, in revealing and investigating accretion processes in young embedded Class 0/I disks.

6 Conclusions

We report new ALMA observations of HDO and SO_2 at an ∼50 au angular resolution in the protobinary system SVS13-A. The line spatial distribution and the radial and vertical profiles indicate that HDO and SO_2 are associated with both components of the binary system, VLA4A and VLA4B. We compare the spatial distribution with that of NH_2CHO, which instead mainly traces the VLA4A component, confirming a chemical differentiation around the two protostars. In addition, the channel maps of HDO emission reveal a further component at blue-shifted velocities (+2.42–4.39 km s^{-1}) spatially coincident with the dust-accretion streamer. The streamer traced by HDO is located at a distance ≥120 au from the VLA4A and VLA4B protostars. Formamide is also detected at the same spatial position. In order to investigate the origin of the molecular emission in the streamer, we evaluate the thermal sublimation temperatures of deuterated water, SO_2 and formamide, using updated BE distributions. We find that a thermal sublimation origin of the molecular emission is excluded, unless the VLA4A source is currently experiencing an accretion burst. Alternatively, the emission morphology is consistent with an accretion shock, produced by an accretion streamer impacting the VLA4A disk, as previously found in more evolved proto-planetary disks. Finally, water has a key role in the planet formation process and it is relevant to investigate its abundance across the different evolutionary stages. The spatial distribution of HDO in SVS13-A demonstrates that in Class I disks water is not necessarily confined in the inner 10 au, as suggested by previous ALMA and NOEMA $H_2{}^{18}O$ observations in 5 Class I disks.[56] In this respect, accretion processes are a powerful tool to investigate the amount of water present in the young disks that will be eventually inherited from the forming planetary systems.

Conflicts of interest

There are no conflicts to declare.

Acknowledgements

This project has received funding from: (1) the Deutsche Forschungsgemeinschaft (DFG, German Research Foundation) under Germany's Excellence Strategy – EXC 2094 – 390783311; (2) the European Research Council (ERC) under the European Union's Horizon 2020 Research and Innovation Program, for the Project “The Dawn of Organic Chemistry” (DOC), grant agreement No 741002; (3) the PRIN-INAF 2016 The Cradle of Life – GENESIS-SKA (GEneral coNditions in Early planetary Systems for the rISe of life with SKA); and (4) the European Union's Horizon 2020 Research and Innovation Programs under projects “Astro-Chemistry Origins” (ACO), Grant No. 811312. This paper makes use of the following ALMA data: ADS/JAO.ALMA#2018.1.01461.S. ALMA is a partnership of the ESO (representing its member states), NSF (USA) and NINS (Japan), together with the NRC (Canada), MOST and ASIAA (Taiwan), and the KASI (Republic of Korea), in cooperation with the Republic of Chile. The Joint ALMA Observatory is operated by the ESO, AUI/NRAO and NAOJ. Most of the computations presented in this paper were performed using the GRICAD infrastructure (**https://gricad.univ-grenoble-alpes.fr**), which is partly supported by the Equip@Meso project (reference ANR-10-EQPX-29-01) of the programme Investissements d'Avenir supervised by the Agence Nationale pour la Recherche. Software: Astropy[57,58] and Matplotlib.[59]

Notes and references

1 E. Bianchi, A. López-Sepulcre, C. Ceccarelli, C. Codella, L. Podio, M. Bouvier and J. Enrique-Romero, *Astrophys. J., Lett.*, 2022, **928**, L3.

2 ALMA Partnership, C. L. Brogan, L. M. Pérez, T. R. Hunter, W. R. F. Dent, A. S. Hales, R. E. Hills, S. Corder, E. B. Fomalont, C. Vlahakis, Y. Asaki, D. Barkats, A. Hirota, J. A. Hodge, C. M. V. Impellizzeri, R. Kneissl, E. Liuzzo, R. Lucas, N. Marcelino, S. Matsushita, K. Nakanishi, N. Phillips, A. M. S. Richards, I. Toledo, R. Aladro, D. Broguiere, J. R. Cortes, P. C. Cortes, D. Espada, F. Galarza, D. Garcia-Appadoo, L. Guzman-Ramirez, E. M. Humphreys, T. Jung, S. Kameno, R. A. Laing, S. Leon, G. Marconi, A. Mignano, B. Nikolic, L.-A. Nyman, M. Radiszcz, A. Remijan, J. A. Rodón, T. Sawada, S. Takahashi, R. P. J. Tilanus, B. Vila Vilaro, L. C. Watson, T. Wiklind, E. Akiyama, E. Chapillon, I. de Gregorio-Monsalvo, J. Di Francesco, F. Gueth, A. Kawamura, C.-F. Lee, Q. Nguyen Luong, J. Mangum, V. Pietu, P. Sanhueza, K. Saigo, S. Takakuwa, C. Ubach, T. van Kempen, A. Wootten, A. Castro-Carrizo, H. Francke, J. Gallardo, J. Garcia, S. Gonzalez, T. Hill, T. Kaminski, Y. Kurono, H.-Y. Liu, C. Lopez, F. Morales, K. Plarre, G. Schieven, L. Testi, L. Videla, E. Villard, P. Andreani, J. E. Hibbard and K. Tatematsu, *Astrophys. J., Lett.*, 2015, **808**, L3.

3 P. D. Sheehan, J. J. Tobin, S. Federman, S. T. Megeath and L. W. Looney, *Astrophys. J.*, 2020, **902**, 141.

4 D. M. Segura-Cox, A. Schmiedeke, J. E. Pineda, I. W. Stephens, M. Fernández-López, L. W. Looney, P. Caselli, Z.-Y. Li, L. G. Mundy, W. Kwon and R. J. Harris, *Nature*, 2020, **586**, 228–231.

5 Ł. Tychoniec, J. J. Tobin, A. Karska, C. Chandler, M. M. Dunham, R. J. Harris, K. M. Kratter, Z.-Y. Li, L. W. Looney, C. Melis, L. M. Pérez, S. I. Sadavoy, D. Segura-Cox and E. F. van Dishoeck, *Astrophys. J., Suppl. Ser.*, 2018, **238**, 19.

6 A. Miotello, I. Kamp, T. Birnstiel, L. I. Cleeves and A. Kataoka, *arXiv*, 2022, arXiv:2203.09818, DOI: **10.48550/arXiv.2203.09818**.

7 P. D. Sheehan, J. J. Tobin, L. W. Looney and S. T. Megeath, *Astrophys. J.*, 2022, **929**, 76.

8 K. I. Öberg and E. A. Bergin, *Phys. Rep.*, 2021, **893**, 1–48.

9 C. Ceccarelli, C. Codella, N. Balucani, D. Bockelée-Morvan, E. Herbst, C. Vastel, P. Caselli, C. Favre, B. Lefloch and K. Öberg, *arXiv*, 2022, arXiv:2206.13270, DOI: **10.48550/arXiv.2206.13270**.

10 E. Herbst and E. F. van Dishoeck, *Annu. Rev. Astron. Astrophys.*, 2009, **47**, 427–480.

11 C. Zucker, E. F. Schlafly, J. S. Speagle, G. M. Green, S. K. N. Portillo, D. P. Finkbeiner and A. A. Goodman, *Astrophys. J.*, 2018, **869**, 83.

12 E. Fiorellino, C. F. Manara, B. Nisini, S. Ramsay, S. Antoniucci, T. Giannini, K. Biazzo, J. Alcalà and D. Fedele, *Astron. Astrophys.*, 2021, **650**, A43.

13 B. Reipurth, R. Chini, E. Krugel, E. Kreysa and A. Sievers, *Astron. Astrophys.*, 1993, **273**, 221–238.

14 B. Lefloch, A. Castets, J. Cernicharo, W. D. Langer and R. Zylka, *Astron. Astrophys.*, 1998, **334**, 269–279.

15 C. Lefèvre, S. Cabrit, A. J. Maury, F. Gueth, B. Tabone, L. Podio, A. Belloche, C. Codella, S. Maret, S. Anderl, P. André and P. Hennebelle, *Astron. Astrophys.*, 2017, **604**, L1.

16 G. Anglada, L. F. Rodríguez and J. M. Torrelles, *Astrophys. J., Lett.*, 2000, **542**, L123–L126.

17 C. Carrasco-González, G. Anglada, L. F. Rodríguez, J. M. Torrelles and M. Osorio, *Astron. J.*, 2008, **136**, 2238–2243.

18 A. K. Diaz-Rodriguez, G. Anglada, G. Blázquez-Calero, M. Osorio, J. F. Gómez, G. A. Fuller, R. Estalella, J. M. Torrelles, S. Cabrit, L. F. Rodríguez, C. Lefèvre, E. Macías, C. Carrasco-González, L. A. Zapata, I. de Gregorio-Monsalvo and P. T. P. Ho, *Astrophys. J.*, 2022, **930**, 91.

19 L. F. Rodríguez, G. Anglada and S. Curiel, *Astrophys. J., Lett.*, 1997, **480**, L125–L128.

20 J. J. Tobin, L. W. Looney, Z.-Y. Li, C. J. Chandler, M. M. Dunham, D. Segura-Cox, S. I. Sadavoy, C. Melis, R. J. Harris, K. Kratter and L. Perez, *Astrophys. J.*, 2016, **818**, 73.

21 K. W. Hodapp and R. Chini, *Astrophys. J.*, 2014, **794**, 169.

22 S. Cazaux, A. G. G. M. Tielens, C. Ceccarelli, A. Castets, V. Wakelam, E. Caux, B. Parise and D. Teyssier, *Astrophys. J., Lett.*, 2003, **593**, L51–L55.

23 E. Bianchi, C. Codella, C. Ceccarelli, F. Vazart, R. Bachiller, N. Balucani, M. Bouvier, M. De Simone, J. Enrique-Romero, C. Kahane, B. Lefloch, A. López-Sepulcre, J. Ospina-Zamudio, L. Podio and V. Taquet, *Mon. Not. R. Astron. Soc.*, 2019, **483**, 1850–1861.

24 C. Codella, C. Ceccarelli, E. Bianchi, L. Podio, R. Bachiller, B. Lefloch, F. Fontani, V. Taquet and L. Testi, *Mon. Not. R. Astron. Soc.*, 2016, **462**, L75–L79.

25 M. De Simone, C. Codella, L. Testi, A. Belloche, A. J. Maury, S. Anderl, P. André, S. Maret and L. Podio, *Astron. Astrophys.*, 2017, **599**, A121.

26 B. Lefloch, R. Bachiller, C. Ceccarelli, J. Cernicharo, C. Codella, A. Fuente, C. Kahane, A. López-Sepulcre, M. Tafalla, C. Vastel, E. Caux, M. González-García, E. Bianchi, A. Gómez-Ruiz, J. Holdship, E. Mendoza, J. Ospina-Zamudio, L. Podio, D. Quénard, E. Roueff, N. Sakai, S. Viti, S. Yamamoto, K. Yoshida, C. Favre, T. Monfredini, H. M. Quitián-Lara, N. Marcelino, H. M. Boechat-Roberty and S. Cabrit, *Mon. Not. R. Astron. Soc.*, 2018, **477**, 4792–4809.

27 A. Belloche, A. J. Maury, S. Maret, S. Anderl, A. Bacmann, P. André, S. Bontemps, S. Cabrit, C. Codella, M. Gaudel, F. Gueth, C. Lefèvre, B. Lefloch, L. Podio and L. Testi, *Astron. Astrophys.*, 2020, **635**, A198.

28 C. Ceccarelli, P. Caselli, F. Fontani, R. Neri, A. López-Sepulcre, C. Codella, S. Feng, I. Jiménez-Serra, B. Lefloch, J. E. Pineda, C. Vastel, F. Alves, R. Bachiller, N. Balucani, E. Bianchi, L. Bizzocchi, S. Bottinelli, E. Caux, A. Chacón-Tanarro, R. Choudhury, A. Coutens, F. Dulieu, C. Favre, P. Hily-Blant, J. Holdship, C. Kahane, A. Jaber Al-Edhari, J. Laas, J. Ospina, Y. Oya, L. Podio, A. Pon, A. Punanova, D. Quenard, A. Rimola, N. Sakai, I. R. Sims, S. Spezzano, V. Taquet, L. Testi, P. Theulé, P. Ugliengo, A. I. Vasyunin, S. Viti, L. Wiesenfeld and S. Yamamoto, *Astrophys. J.*, 2017, **850**, 176.

29 Y.-L. Yang, N. Sakai, Y. Zhang, N. M. Murillo, Z. E. Zhang, A. E. Higuchi, S. Zeng, A. López-Sepulcre, S. Yamamoto, B. Lefloch, M. Bouvier, C. Ceccarelli, T. Hirota, M. Imai, Y. Oya, T. Sakai and Y. Watanabe, *Astrophys. J.*, 2021, **910**, 20.

30 J. P. McMullin, B. Waters, D. Schiebel, W. Young and K. Golap, in *CASA Architecture and Applications*, ed. R. A. Shaw, F. Hill and D. J. Bell, 2007, vol. 376, p. 127.
31 J. K. Messer, F. C. De Lucia and P. Helminger, *J. Mol. Spectrosc.*, 1984, **105**, 139–155.
32 H. M. Pickett, R. L. Poynter, E. A. Cohen, M. L. Delitsky, J. C. Pearson and H. S. P. Müller, *J. Quant. Spectrosc. Radiat. Transfer*, 1998, **60**, 883–890.
33 H. S. P. Müller, F. Schlöder, J. Stutzki and G. Winnewisser, *J. Mol. Struct.*, 2005, **742**, 215–227.
34 S. G. Kukolich and A. C. Nelson, *Chem. Phys. Lett.*, 1971, **11**, 383–384.
35 C. Ceccarelli, P. Caselli, D. Bockelée-Morvan, O. Mousis, S. Pizzarello, F. Robert and D. Semenov, *Protostars and Planets VI*, 2014, pp. 859–882.
36 R. T. Garrod, S. L. Widicus Weaver and E. Herbst, *Astrophys. J.*, 2008, **682**, 283–302.
37 D. Skouteris, F. Vazart, C. Ceccarelli, N. Balucani, C. Puzzarini and V. Barone, *Mon. Not. R. Astron. Soc.*, 2017, **468**, L1–L5.
38 A. Fuente, P. Rivière-Marichalar, L. Beitia-Antero, P. Caselli, V. Wakelam, G. Esplugues, M. Rodríguez-Baras, D. Navarro-Almaida, M. Gerin, C. Kramer, R. Bachiller, J. R. Goicoechea, I. Jiménez-Serra, J. C. Loison, A. Ivlev, R. Martín-Doménech, S. Spezzano, O. Roncero, G. Muñoz-Caro, S. Cazaux and N. Marcelino, *arXiv*, 2022, arXiv:2212.03742, DOI: **10.48550/arXiv.2212.03742**.
39 M. Minissale, Y. Aikawa, E. Bergin, M. Bertin, W. A. Brown, S. Cazaux, S. B. Charnley, A. Coutens, H. M. Cuppen, V. Guzman, H. Linnartz, M. R. S. McCoustra, A. Rimola, J. G. M. Schrauwen, C. Toubin, P. Ugliengo, N. Watanabe, V. Wakelam and F. Dulieu, *ACS Earth Space Chem.*, 2022, **6**, 597–630.
40 S. Ferrero, F. Grieco, A. S. Ibrahim Mohamed, F. Dulieu, A. Rimola, C. Ceccarelli, C. Nervi, M. Minissale and P. Ugliengo, *Mon. Not. R. Astron. Soc.*, 2022, **516**, 2586–2596.
41 S. Ferrero, L. Zamirri, C. Ceccarelli, A. Witzel, A. Rimola and P. Ugliengo, *Astrophys. J.*, 2020, **904**, 11.
42 J. Perrero, J. Enrique-Romero, S. Ferrero, C. Ceccarelli, L. Podio, C. Codella, A. Rimola and P. Ugliengo, *Astrophys. J.*, 2022, **938**, 158.
43 S. L. Tait, Z. Dohnálek, C. T. Campbell and B. D. Kay, *J. Chem. Phys.*, 2005, **122**, 164708.
44 E. Bianchi, C. Ceccarelli, C. Codella, A. López-Sepulcre, S. Yamamoto, N. Balucani, P. Caselli, L. Podio, R. Neri, R. Bachiller, C. Favre, F. Fontani, B. Lefloch, N. Sakai and D. Segura-Cox, *Astron. Astrophys.*, 2022, **662**, A103.
45 L. Tinacci, A. Germain, S. Pantaleone, S. Ferrero, C. Ceccarelli and P. Ugliengo, *ACS Earth Space Chem.*, 2022, **6**, 1514–1526.
46 L. Podio, B. Tabone, C. Codella, F. Gueth, A. Maury, S. Cabrit, B. Lefloch, S. Maret, A. Belloche, P. André, S. Anderl, M. Gaudel and L. Testi, *Astron. Astrophys.*, 2021, **648**, A45.
47 C. Ceccarelli, A. Castets, E. Caux, D. Hollenbach, L. Loinard, S. Molinari and A. G. G. M. Tielens, *Astron. Astrophys.*, 2000, **355**, 1129–1137.
48 T.-H. Hsieh, N. M. Murillo, A. Belloche, N. Hirano, C. Walsh, E. F. van Dishoeck, J. K. Jørgensen and S.-P. Lai, *Astrophys. J.*, 2019, **884**, 149.

49 J.-E. Lee, S. Lee, G. Baek, Y. Aikawa, L. Cieza, S.-Y. Yoon, G. Herczeg, D. Johnstone and S. Casassus, *Nat. Astron*, 2019, **3**, 314–319.

50 M. R. Bate and I. A. Bonnell, *Mon. Not. R. Astron. Soc.*, 1997, **285**, 33–48.

51 S. Ceppi, N. Cuello, G. Lodato, C. Clarke, C. Toci and D. J. Price, *Mon. Not. R. Astron. Soc.*, 2022, **514**, 906–919.

52 A. Garufi, L. Podio, C. Codella, D. Segura-Cox, M. Vander Donckt, S. Mercimek, F. Bacciotti, D. Fedele, M. Kasper, J. E. Pineda, E. Humphreys and L. Testi, *Astron. Astrophys.*, 2022, **658**, A104.

53 K. Kratter and G. Lodato, *Annu. Rev. Astron. Astrophys.*, 2016, **54**, 271–311.

54 M. J. Maureira, M. Gong, J. E. Pineda, H. B. Liu, K. Silsbee, P. Caselli, J. Zamponi, D. M. Segura-Cox and A. Schmiedeke, *Astrophys. J., Lett.*, 2022, **941**, L23.

55 T. H. Hsieh, D. M. Segura-Cox, J. E. Pineda, P. Caselli, L. Bouscasse, R. Neri, A. Lopez-Sepulcre, M. T. Valdivia-Mena, M. J. Maureira, T. Henning, G. V. Smirnov-Pinchukov, D. Semenov, T. Möller, N. Cunningham, A. Fuente, S. Marino, A. Dutrey, M. Tafalla, E. Chapillon, C. Ceccarelli and B. Zhao, *Astron. Astrophys.*, 2023, **669**, A137.

56 D. Harsono, M. V. Persson, A. Ramos, N. M. Murillo, L. T. Maud, M. R. Hogerheijde, A. D. Bosman, L. E. Kristensen, J. K. Jørgensen, E. A. Bergin, R. Visser, J. C. Mottram and E. F. van Dishoeck, *Astron. Astrophys.*, 2020, **636**, A26.

57 Astropy Collaboration, T. P. Robitaille, E. J. Tollerud, P. Greenfield, M. Droettboom, E. Bray, T. Aldcroft, M. Davis, A. Ginsburg, A. M. Price-Whelan, W. E. Kerzendorf, A. Conley, N. Crighton, K. Barbary, D. Muna, H. Ferguson, F. Grollier, M. M. Parikh, P. H. Nair, H. M. Unther, C. Deil, J. Woillez, S. Conseil, R. Kramer, J. E. H. Turner, L. Singer, R. Fox, B. A. Weaver, V. Zabalza, Z. I. Edwards, K. A. Bostroem, D. J. Burke, A. R. Casey, S. M. Crawford, N. Dencheva, J. Ely, T. Jenness, K. Labrie, P. L. Lim, F. Pierfederici, A. Pontzen, A. Ptak, B. Refsdal, M. Servillat and O. Streicher, *Astron. Astrophys.*, 2013, **558**, A33.

58 Astropy Collaboration, A. M. Price-Whelan, B. M. Sipőcz, H. M. Günther, P. L. Lim, S. M. Crawford, S. Conseil, D. L. Shupe, M. W. Craig, N. Dencheva, A. Ginsburg, J. T. VanderPlas, L. D. Bradley, D. Pérez-Suárez, M. de Val-Borro, T. L. Aldcroft, K. L. Cruz, T. P. Robitaille, E. J. Tollerud, C. Ardelean, T. Babej, Y. P. Bach, M. Bachetti, A. V. Bakanov, S. P. Bamford, G. Barentsen, P. Barmby, A. Baumbach, K. L. Berry, F. Biscani, M. Boquien, K. A. Bostroem, L. G. Bouma, G. B. Brammer, E. M. Bray, H. Breytenbach, H. Buddelmeijer, D. J. Burke, G. Calderone, J. L. Cano Rodríguez, M. Cara, J. V. M. Cardoso, S. Cheedella, Y. Copin, L. Corrales, D. Crichton, D. D'Avella, C. Deil, É. Depagne, J. P. Dietrich, A. Donath, M. Droettboom, N. Earl, T. Erben, S. Fabbro, L. A. Ferreira, T. Finethy, R. T. Fox, L. H. Garrison, S. L. J. Gibbons, D. A. Goldstein, R. Gommers, J. P. Greco, P. Greenfield, A. M. Groener, F. Grollier, A. Hagen, P. Hirst, D. Homeier, A. J. Horton, G. Hosseinzadeh, L. Hu, J. S. Hunkeler, Ž. Ivezić, A. Jain, T. Jenness, G. Kanarek, S. Kendrew, N. S. Kern, W. E. Kerzendorf, A. Khvalko, J. King, D. Kirkby, A. M. Kulkarni, A. Kumar, A. Lee, D. Lenz, S. P. Littlefair, Z. Ma, D. M. Macleod, M. Mastropietro, C. McCully, S. Montagnac, B. M. Morris, M. Mueller, S. J. Mumford, D. Muna, N. A. Murphy, S. Nelson, G. H. Nguyen, J. P. Ninan, M. Nöthe, S. Ogaz, S. Oh, J. K. Parejko, N. Parley, S. Pascual, R. Patil, A. A. Patil, A. L. Plunkett, J. X. Prochaska, T. Rastogi, V. Reddy Janga,

J. Sabater, P. Sakurikar, M. Seifert, L. E. Sherbert, H. Sherwood-Taylor, A. Y. Shih, J. Sick, M. T. Silbiger, S. Singanamalla, L. P. Singer, P. H. Sladen, K. A. Sooley, S. Sornarajah, O. Streicher, P. Teuben, S. W. Thomas, G. R. Tremblay, J. E. H. Turner, V. Terrón, M. H. van Kerkwijk, A. de la Vega, L. L. Watkins, B. A. Weaver, J. B. Whitmore, J. Woillez and V. Zabalza, *Astron. J.*, 2018, **156**, 123.
59 J. D. Hunter, *Comput. Sci. Eng.*, 2007, **9**, 90–95.

